processes

MDPI

Article

Thermodynamic Justification for the Effectiveness of the Oxidation—Soda Conversion of Ilmenite Concentrates

Kuralay Akhmetova, Nesipbay Tusupbayev, Bagdaulet Kenzhaliyev, Sergey Gladyshev, Nazym Akhmadiyeva * and Leila Imangaliyeva

Institute of Metallurgy and Ore Beneficiation, Satbayev University, Almaty 050010, Kazakhstan; kuralai-1950@mail.ru (K.A.); nesipbay@mail.ru (N.T.); bagdaulet_k@mail.ru (B.K.); gladyshev.sergey55@mail.ru (S.G.); leila.imangalieva@mail.ru (L.I.)

* Correspondence: akhmadiyeva141@gmail.com

Abstract: This article presents the results of a thermodynamic analysis of the oxidation soda conversion reactions of minerals in ilmenite concentrates in the temperature range of 373–2273 K. The thermodynamic parameters of pseudorutile, pseudobrukite, and the new minerals, zhikinite and spessartine, were calculated for the first time. It has been established that the most important criterion relating to the stability of titanium minerals and related elements, as well as the reaction properties of the structural oxides of metals and silicon, is their degree of oxidation. Oxides of silicon (IV) and manganese have the best reactivity in solid-phase oxidizing alkaline environments (VI). Modeling this process scientifically substantiates the mechanism involved in the destruction of minerals in ilmenite concentrates in the low-temperature region in the presence of atmospheric oxygen and sodium oxide of soda ash, which are decomposed through the absorption of heat and the evaporation of moisture during the dehydration of hydrated minerals of iron and manganese and the dehydration of the soda–ilmenite batch. Tests conducted during pilot metallurgical production at the Institute of Metallurgy and Enrichment (PMP of JSC) confirmed the feasibility of processing high-chromium and siliceous rutile leucoxene ilmenite concentrates, which are unsuitable for traditional pyro- and hydro-metallurgical enrichment methods, through single-stage oxidation soda roasting, followed by the leaching of easily soluble sodium salts of iron and associated impurities with water and a dilute hydrochloric acid solution. The proposed energy-saving method ensures the production of high-purity (>98%) synthetic rutile while eliminating the formation of strong deposits on the lining of roasting units.

Keywords: ilmenite concentrate; oxidation soda conversion; thermodynamics; synthetic rutile

check for updates

Citation: Akhmetova, K.; Tusupbayev, N.; Kenzhaliyev, B.; Gladyshev, S.; Akhmadiyeva, N.; Imangaliyeva, L. Thermodynamic Justification for the Effectiveness of the Oxidation—Soda Conversion of Ilmenite Concentrates. *Processes* **2024**, *12*, 2276. https://doi.org/10.3390/pr12102276

Academic Editor: Francisco José Hernández Fernández

Received: 23 August 2024
Revised: 14 October 2024
Accepted: 15 October 2024
Published: 18 October 2024

Copyright: © 2024 by the authors. Licensee MDPI, Basel, Switzerland. This article is an open access article distributed under the terms and conditions of the Creative Commons Attribution (CC BY) license (https://creativecommons.org/licenses/by/4.0/).

1. Introduction

Mineral deposits of titanium are widespread globally; however, reserves of economically valuable rutile sand ores and high-quality ilmenite sands are limited [1]. According to current estimates, the total world reserves of titanium in ilmenite and rutile combined in 2023 were approximately 745 million metric tons. Moreover, ilmenite accounts for 94% of the world's titanium reserves, with the remainder in rutile [2]. The bulk (up to 95%) of the annually mined ilmenite raw material is used to produce titanium dioxide. The compound annual growth rate of the titanium dioxide market supplied to manufacturers of white titanium pigments is projected to be 8.9% from 2023 to 2032 [3].

The complexity of the material composition of hard-to-enrich ilmenite concentrates limits the effectiveness of commercial methods used to produce synthetic rutile and electrothermal titanium slags. Numerous studies focused on the processing of ilmenite concentrates are mainly devoted to carbothermal smelting with and without flux additives, particularly soda [4].

Titanium slags obtained as a result of carbothermal smelting are heavily contaminated with impurities, and refinement methods involving sulfuric acid result in the formation of

a large volume of sulfate iron, leading to the excessively high consumption of acid during chlorination [5]. The number of raw materials suitable for the hydrochloric acid leaching of titanium slags is limited; therefore, they have not found industrial applications [6]. The Benelite process, designed for the refinement of ilmenite sands containing a high content of titanium dioxide and a low iron oxide content, becomes technically unsuitable when the concentration of chromium and magnesium exceeds the permissible concentration, suppressing the slow rate of aeration leaching [6]. The Altair process is low-yielding and unprofitable due to the multi-stage leaching, conversion, and separation of metals. In addition to the technique of processing ilmenite concentrates using carbo-thermal smelting, other known methods include oxidation–reduction roasting [7].

In particular, the sulfate method used for the production of titanium dioxide through rutile and anatase modification is not suitable for processing leucoxene ilmenite concentrates containing rutile that is insoluble in acids. The enrichment process used for ilmenite sand concentrates with a high content of titanium dioxide and a low content of iron oxide is technically unacceptable when the permissible concentrations of magnesium and chromium are exceeded. This is due to the suppression of the slow aeration leaching of metallic iron when using ammonium chloride solution [8]. The ERMS SR technology used for the production of high-purity synthetic rutile (>97%), developed by the Australian company Austpac Resources, includes a two-stage redox roasting of the heavy mineral concentrate with intermediate magnetic separation [9]. The technology for producing UGS (upgraded titania slag) matches the quality (94–95% TiO_2) of synthetic rutile by using the energy-consuming double thermal oxidation–reduction process with intermediate magnetic separation, as developed by the Canadian company QIT-Fer & Titane Inc. (Havre-Saint-Pierre, QC, Canada) [10,11]. These are not applicable for processing rutilized ilmenite concentrates due to the inability to separate rutile from rock-forming vein minerals using magnetic separation.

An attractive method for synthetic rutile production is a one-stage oxidizing soda process involving the conversion of polymineral ilmenite concentrates and the enrichment of titanium slags. Morsi et al. [12] determined the possibility of completely extracting titanium dioxide by sintering ilmenite ore with a molar ratio of sodium oxide to titanium dioxide of 2.5, followed by roasting at 1000 °C, 1100 °C, or 1200 °C for 120, 60, or 30 min, respectively. They reported that higher sodium titanates of $Na_8Ti_5O_{14}$ and $Na_6Ti_2O_7$ formed during the sintering process turn into lower-sodium titanates, which can be easily soluble in dilute sulfuric acid and easily separated from iron. Lasheen [13] determined the possibility of modifying titanium slag smelted from Rosetta ilmenite concentrate by roasting with soda ash at an optimal ratio of Na_2CO_3 and slag equal to 0.55:1 at a temperature of 850 °C for 0.5 h. Nafeaa et al. [14] found that the degree of conversion of granular and powdered Rosetta ilmenite concentrate, determined by analyzing the composition of the resulting sodium titanates, increases with increasing roasting temperature in air and the percentage of soda ash in the concentrate. Abhishek [15] studied the oxidative roasting of Bomar ilmenite with soda ash in the temperature range of 873–1173 K, concluding that the process proceeds in two stages—with the formation of sodium titanate and ferruginous sodium titanate in the first stage, followed by the decomposition of ferruginous sodium titanate with the formation of sodium ferrite and titanium dioxide in the second stage—assuming that divalent iron ions are replaced by sodium soda ions as a result of diffusion from the ilmenite crystal lattice.

The relevance of such research lies in the limited reserves of economically valuable rutile sand ores and high-quality ilmenite sands, increasing consumption, and the need to increase the production capacity of synthetic rutile, necessitating the processing of ilmenite concentrates with complex material compositions.

The results of our fundamental research clarify the real decomposition mechanisms of valuable titanium ore minerals and related elements under the action of oxygen and soda ash, confirming the feasibility of processing high-chromium and -silica rutilized leucoxene ilmenite concentrates—which are unsuitable for processing when using traditional pyro-

and hydro-metallurgical methods of enrichment—using oxidative soda conversion. These results are presented below [16].

2. Materials and Methods

2.1. Thermodynamic Analysis

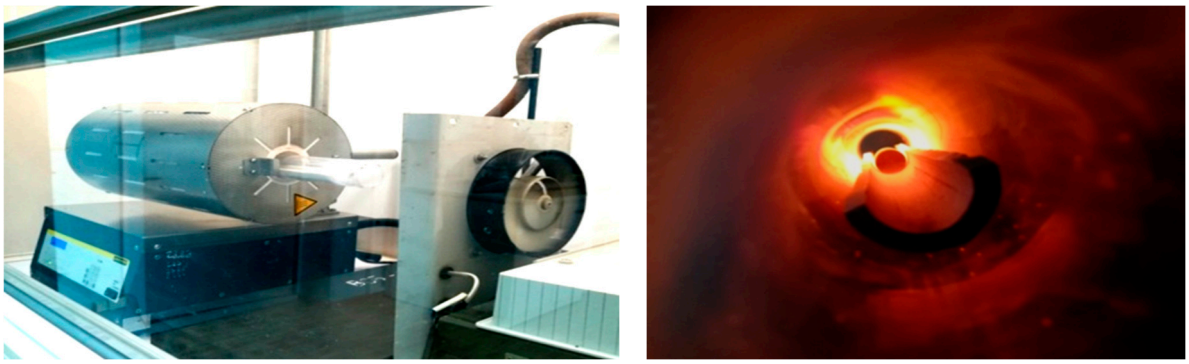
The numerical values relating to the thermal effects of the separate and total reactions of mineral decomposition for a representative batch of ilmenite concentrate from an Obukhov deposit were determined. This calculation considered the heat capacity ΔC°_{p} of reacting substances and the formed products and involved computing the enthalpy ΔH°_{T}, entropy ΔS°_{T}, and Gibbs energy ΔG°_{T} in each temperature interval from 373 to 2273 K, using reference standard thermodynamic values at 298 K [17]. Due to the absence in the literature of standard thermodynamic values of ΔH°_{298}, ΔS°_{298}, and ΔC°_{298} for minerals, such as spessartine $Mn_3Al_2[SiO_4]_3$, pseudorutile $Fe_2Ti_3O_9$, and pseudobrukite $FeTi_2O_5$, these values were determined using the incremental Kumok method, the additive Neumann–Kopp rule, and the Mostafa group contribution method [18]. Thermodynamic calculations of chemical reactions were additionally verified using the HSC Chemistry 8.0 (2014) program.

2.2. Physicochemical and Experimental Studies

The phase composition of the Obukhovskoye ilmenite concentrate provided by the Thioline Mining and Processing Company was analyzed through classification on a vibratory shaker with a set of sieve webs with different mesh sizes. The mineral composition of the concentrate was identified using a D8 Advance (BRUKER) X-ray diffractometer with Cu-Ka emission. Thermal analysis was performed using an STA 449 F3 Jupiter synchronous thermal analyzer (Munchen, Germany) with NETZSCH Proteus software v.7.1, applying a linear heating rate of 15 °C/min in a highly purified argon atmosphere with a linear cooling rate of 17 °C/min to 500 °C [19]. Local areas of polished samples, sputtered with a thin layer of graphite for contrast surface display, were analyzed using a JEOLJXA-8230 scanning electron-probe microanalyzer from JEOL (Japan, Tokyo). The chemical composition of the products was analyzed using an Axios X-ray fluorescence wave-dispersive spectrometer, an Optima 2000 DV "Perkin Elmer Inc." atomic emission spectrometer with inductively coupled plasma (Shelton, CT, USA) and an Agilent 7500 A ICP-MS (Santa Clara, CA, USA) mass spectrometer on the basis of inductively coupled plasma. A "pure analytical reagent" of sodium carbonate was used as a sintering alkaline reagent. The soda–ilmenite charge with the addition of 2% aqueous molasses solution as a binder was briquetted via compaction in a cylindrical steel mold with a diameter of 16 mm on a PSU-10 pressing machine with a pressure force of 50 mPa. The oxidative firing of briquettes of soda–ilmenite charge was carried out in alunda boats placed in a quartz tube with a through hole. Continuous ventilation of the reaction zone was supplied using atmospheric oxygen. A Nabertherm horizontal tubular electric furnace with a B-180 controller for 60–120 min was used when the temperature reached 1100–1200 °C. The soda concentrate charge cake was refined with deionized water, then with 20% hydrochloric acid solution at a solid-to-liquid ratio of 3, a temperature of 90 °C, and a pulp stirring speed of 150 rpm for 1 h in thermostatized beakers heated using a circulating hot water thermostat LT-108 "Loip" (Saint Petersburg, Russia). The alkaline pulp was filtered under a vacuum using a water jet pump through a Buechner funnel with a "blue ribbon" filter, while the acidic pulp was filtered via centrifugation. Washed and dehydrated acid filtrate cakes were calcined at a temperature of 900 °C.

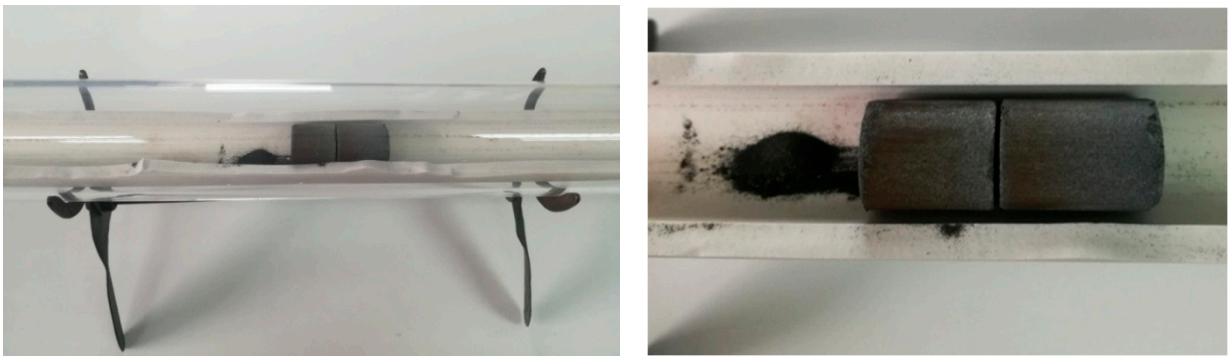
The optimization of the technological conditions established that the oxidative soda conversion of briquetted ilmenite concentrate charge, with an equivalent mass ratio with alkaline reagent at a temperature of 1200 °C for 2 h and subsequent refining of concentrate cinder with water, followed by 20% hydrochloric acid solution at a solid-to-liquid ratio of 1:3 and a temperature of 90 °C for 1 h, provides high-purity synthetic rutile washed with deionized water and calcined at a temperature of 900 °C.

The oxidizing soda conversion of the briquetted concentrate charge to produce porous specks eliminates the formation of strong deposits on the lining of the roasting furnace (Figures 1 and 2).



(**a**) (**b**)

Figure 1. Horizontal roasting tube furnace (**a**) and reaction zone of the furnace with briquette in an alunda boat (**b**).



(**a**) (**b**)

Figure 2. Tray with briquettes cooled in an alunda boat in the air (**a**) and boat containing the cooled briquettes (**b**).

3. Results and Discussion

3.1. Characteristics of Ore Raw Materials and Ilmenite Concentrate

The Obukhovskoye deposit of titanium–zircon sands is located in the Taiyshinskiy district of the North Kazakhstan region. Formed under coastal–marine and partly lagoonal conditions, the deposit belongs to gravel–sandy–clay formations of the Chegan Formation and amounts to 6,150,000 cubic meters. Proven reserves of the most seasoned fine-grained ore sands have the following mineral contents (kg/m^3): ilmenite—82.09; rutile—21.36; leucoxene—5.74; and zircon—80.41. Approximately 80–85% of the useful components of the granular fraction of sands are concentrated in the size class of −0.2 + 0.04 mm. The clay fraction of the sands is represented by particles smaller than 0.02 mm. Ore and rock-forming minerals, in order of decreasing grain size, are arranged in the following sequence: quartz, tourmaline, sillimanite, staurolite, distene, leucoxene, rutile, ilmenite, chromospinelides, and zircon. The high content of basic minerals, the complete absence of mineral aggregates, and the fine-grained nature of ore sands provide the possibility of obtaining ilmenite, rutile, and zircon concentrates. X-ray phase diagnostics of fractional separation products of ilmenite concentrate with grain sizes ranging from +0.071 to −0 mm established the presence of individual and complex minerals of titanium, silicon, zirconium, chromium, and aluminum (Figure 3, Table 1).

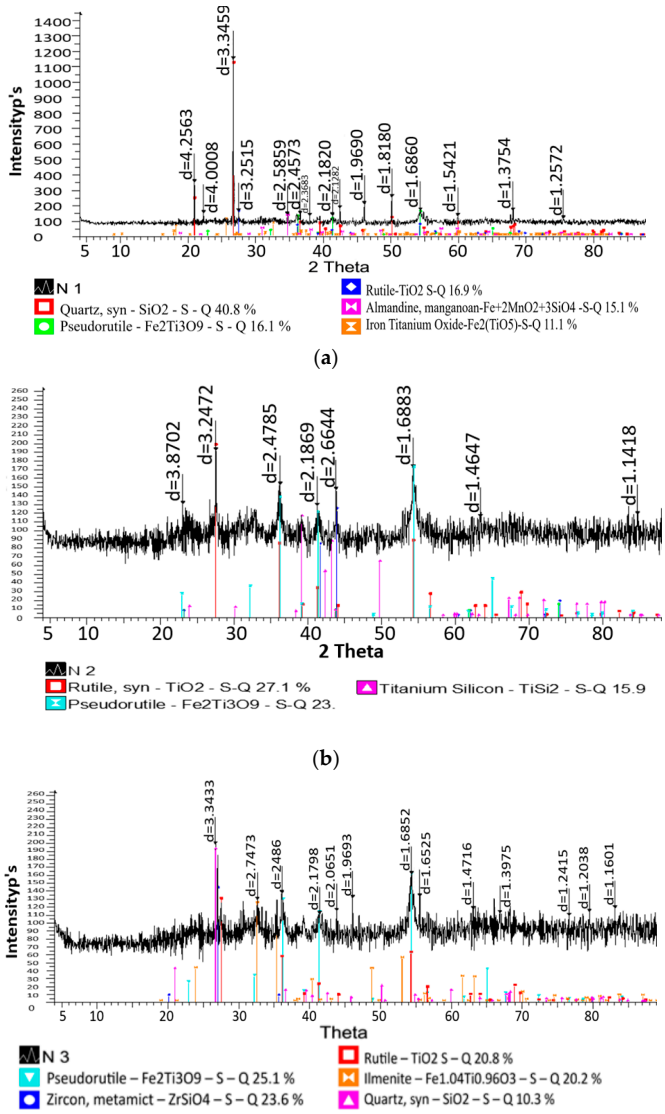


Figure 3. X-ray phase analysis of fractional samples of ilmenite concentrate with grain sizes of −0.071 +0.063 (**a**), −0.063 +0.044 (**b**), and −0.044 +0 (**c**).

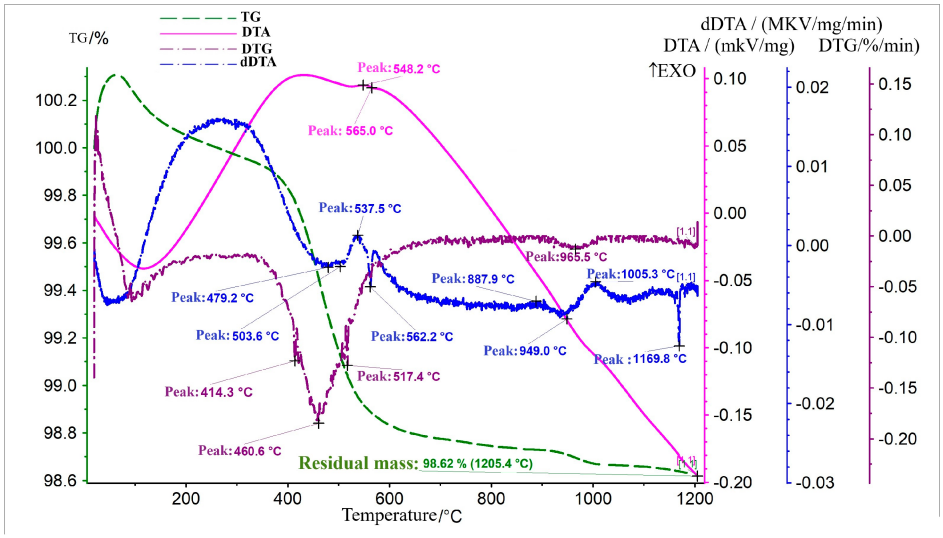
Table 1. Mineral composition of ilmenite concentrate.

Yield, %	Components	Formula	Content, in wt %
Sample size from −0.071 to +0.063 мм (a)			
11.47	Quarts, syn	SiO_2	40.8
	Rutil, syn	TiO_2	16.9
	Pseudorutil	$Fe_2(TiO_3)_3$	16.9
	Pseudobrukite	$Fe_2(TiO_5)$	11.3
	Spessartine	$Mn_3AI_2[SiO_4]_3$	14.2
Sample size from −0.063 to +0.044 мм (b)			
88.53	Rutil, syn	TiO_2	27.1
	Pseudorutil	$Fe_2(TiO_3)_3$	23.5
	Zhiqinite	$TiSi_2$	15.9
	Aluminian Chomit	$Fe(Cr,Al)_2O_4$	16.6
	Aluminian Manganese	$MnAI_6$	17.0

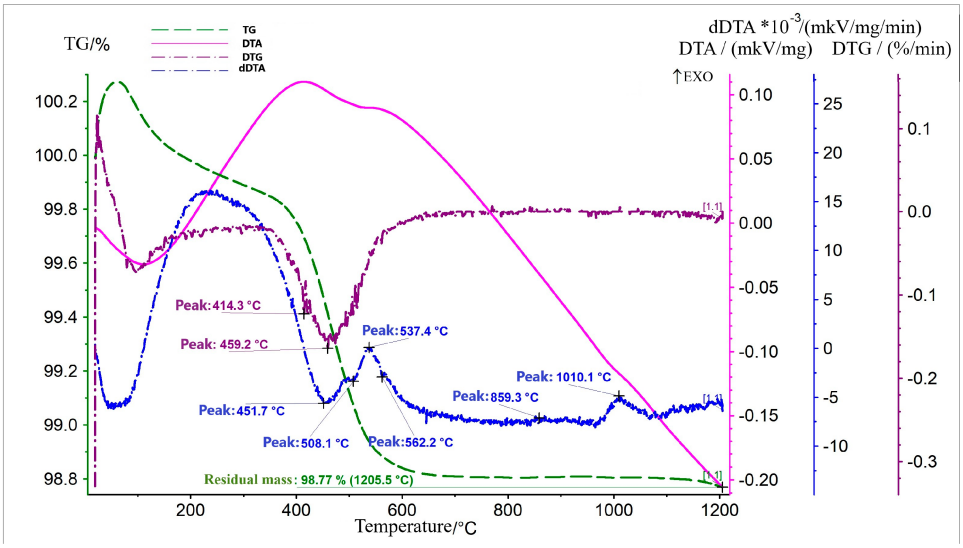
Table 1. *Cont.*

Yield, %	Components	Formula	Content, in wt %
Sample size from +0.071 to −0 мм (c)			
100	Ilmenit	$FeTiO_3$	20.0
	Rutil	TiO_2	20.8
	Pseudorutil	$Fe_2(TiO_3)_3$	25.9
	Zircon, metamict	$ZrSiO_4$	23.0
	Quarts, syn	SiO_2	10.3

Thermal analysis showed the presence of hydrated minerals of iron–lepidocrocite and manganese–manganite (Figure 4).

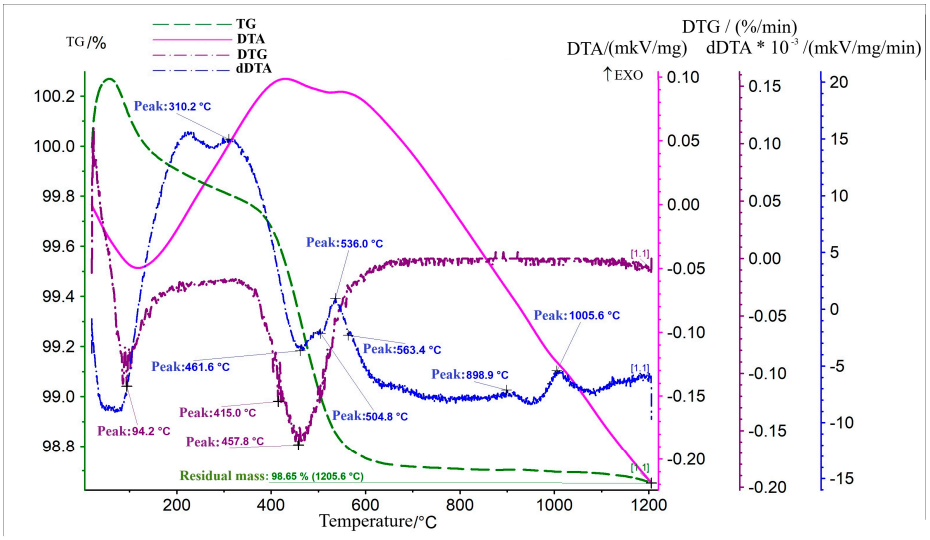


(**a**)



(**b**)

Figure 4. *Cont.*



(**c**)

Figure 4. Thermograms of samples of ilmenite concentrate with grain sizes of −0.071 +0.063 (**a**), −0.063 +0.044 (**b**), and +0.071 −0 (**c**).

The temperature range for the dehydration and phase transformation of lepidocrocite and manganite was determined via the identification of extremes of endo- and exothermic effects on the thermogram curves of dDTA and DTG.

$$\text{Lepidocrocite } \gamma\text{·FeOOH} \xrightarrow{414.3 \div 415\ ^\circ\text{C}} \text{goethite } \alpha\text{·FeOOH} \xrightarrow{457.8 \div 479.2\ ^\circ\text{C}} \text{maghemite } \gamma\text{·}Fe_2O_3 \xrightarrow{536 \div 537.5\ ^\circ\text{C}} \text{hematite } \alpha\text{·}Fe_2O_3 \quad (1)$$

$$\text{Manganite MnOOH} \xrightarrow{479.2\ ^\circ\text{C}} \text{bixbyite } \beta\text{-}Mn_2O_3 \xrightarrow{949 \div 965.5\ ^\circ\text{C}} \text{hausmanite } \beta\text{·}Mn_3O_4 \xrightarrow{1169.8\ ^\circ\text{C}} \gamma\text{·}Mn_3O_4 \quad (2)$$

Enantiotropic polymorphic transformation of quartz

$$\alpha\text{-}SiO_2 \xleftrightarrow{562.2 \div 565\ ^\circ\text{C}} \beta\text{-}SiO_2 \quad (3)$$

Decomposition of ilmenite to form amorphous iron trioxide and titanium dioxide under the action of residual oxygen

$$FeTiO_3 \xrightarrow{310.2 \div 898.9\ ^\circ\text{C}} Fe_2O_3 + TiO_2 \quad (4)$$

Crystallization of rutile and pseudobrukite. (5)

The temperature range and character of phase transformations of ilmenite concentrate minerals under an argon atmosphere are presented in Table 2.

When heating up to a temperature of 1205.4 ÷ 1205.6 °C under an inert gas atmosphere, it was found that mass loss of Obukhov ilmenite concentrate samples does not depend on their grain size (Table 3).

The manifested thermal endothermic effects indicated extremes at temperatures of 479.2 and 517.4 °C, 451.7 and 508.1 °C, and 461.6 and 504.8 °C in fractional samples of concentrate with sizes of −0.071 +0.063 (a), −0.063 + 0.044 (b), and −0.044 + 0 (c), respectively, demonstrating that the decomposition of the minerals present in the concentrate and the formation of new varieties of minerals are accompanied by mass losses of suspensions of the analyzed products.

The chemical composition of the concentrate, in accordance with the mineral composition, is characterized by an abnormally high content of chromium trioxide (Table 4).

Table 2. Temperature range and character of phase transformations of ilmenite concentrate minerals under an argon atmosphere.

Mineral	Formula	Temperature, °C			Processes
		Samples			
		a	b	c	
Goethite	FeO(OH)	479.2 *	459.2 *	457.8 *	Dehydration
Lepidocrocite	γ-FeO(OH)	414.3 *	414.3 *	415 *	Dehydration and formation of γ-Fe_2O_3
		537.5 **	537.4 **	536 **	Transition to α-Fe_2O_3
Manganite	γ-MnO(OH)	479.2 *	–	–	Dehydration and formation of β-Mn_2O_3
		965.5–949 *			Decomposition with oxygen scavenging and formation of β-Mn_3O_4
		1169.8 *			Enantiotropic polymorphic transformation to γ-Mn_3O_4
Ilmenite		887.9 **	853.9 **	310.2 **–898.9 **	Oxidation of Fe^{+2} and formation of amorphous Fe_2O_3 and TiO_2
Rutile Pseudobrookite	TiO_2	1005.3 **	1010.1 **	1005.6 **	Crystallization
Quartz	SiO_2	562.2 *	562.2 *	563.4 *	Enantiotropic polymorphic transformation
Clay mineral		517.4 *	508.1 *	504.8 *	Oxidation

Temperature range: *—endothermic effect; **—exothermic effect.

Table 3. Weight loss of Obukhovskoye ilmenite concentrate samples in argon atmosphere.

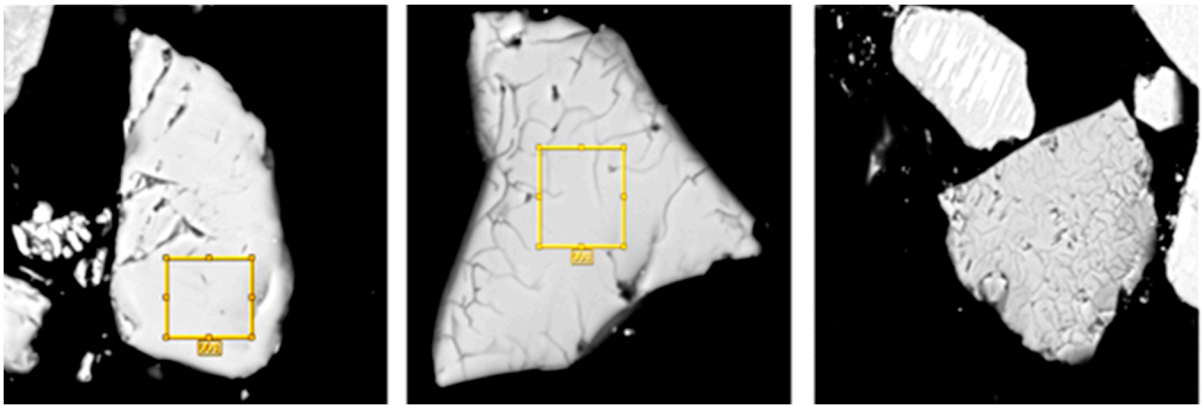
Samples	Coarseness, mm	Initial Mass, g	Residual Mass, %	Weight Loss, %
a	−0.071 +0.063	0.301	98.62	1.38
b	−0.063 +0.044	0.306	98.77	1.23
c	+0.071 −0	0.304	98.65	1.35

Table 4. Chemical compositions of different types of ilmenite concentrates.

Components	Content, in wt %					
	Kazakhstan	Ukraine	Australia [9]	South Africa [20]	Egypt [21]	India [15]
	Obukhovskyi	Volnogorskyi	Capel	Hillendale	Abu Ghalaga	Bomar
TiO_2	51.16	66.8	55.43	48.40	36.78	69.25
FeO	3.15	20.5	22.51	36.15	25.85	15.2
Fe_2O_3	28.78	n/a	18.16	12.29	29.86	6.1
SiO_2	1.8	0.82	1.41	0.44	4.46	3.8
Al_2O_3	2.0	1.8	0.25	0.27	0.72	2.4
Cr_2O_3	7.49	1.5	0.03	0.09	0.21	0.2
CaO	0.1	0.57	n/a	0.02	0.15	0.10
MgO	0.71	0.89	n/a	0.50	0.81	0.9
MnO	1.61	0.85	1.44	1.06	0.36	0.37
V_2O_5	0.18	0.38	0.13	0.25	0.38	-
P_2O_5	0.18	0.25	0.15	0.01	0.03	0.3
ZrO_2	0.41	0.12	0.08	0.08	LOI 0.17	LOI 0.8
	Other 2.43	Other 5.52	Other 0.41	Other 0.44		

Electron probe microscopy of concentrate cinders revealed that, during air firing, the crystal lattice of iron-oxide mineral chromite—which has a dense structure and approximately the same hardness (5.5 on the Mohs scale) as ilmenite—is deformed, and as a result

of oxidation, results in the loosening of divalent iron and the formation of reactive iron trioxide Fe_2O_3 (Figures 5 and 6).

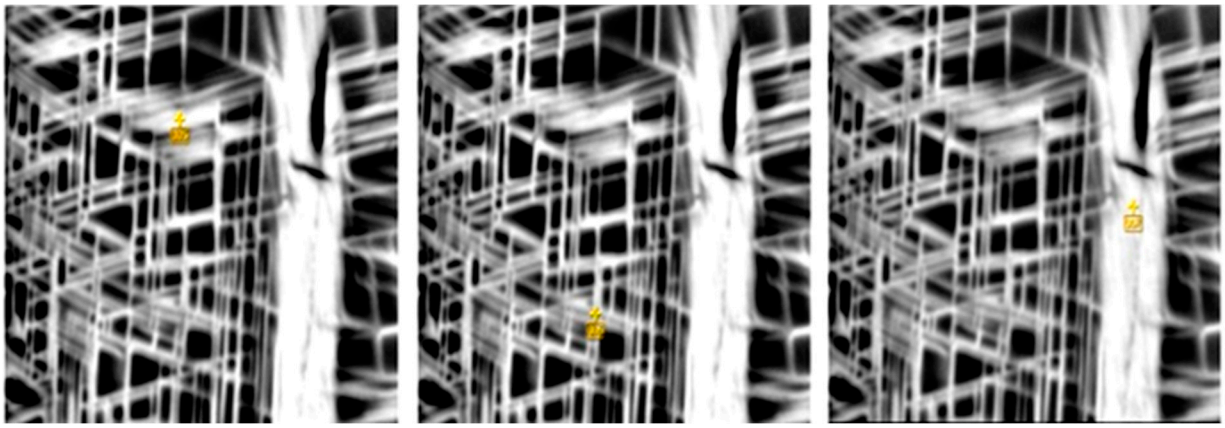


Elements	ms%	mol%
O	33.64	59.69
Mg	4.33	5.06
Al	4.17	4.39
Ti	0.81	0.48
Cr	36.85	20.12
Fe	20.19	10.26
Total	100.00	100.00

Elements	ms%	mol%
O	39.91	60.86
Mg	6.96	6.98
Al	17.66	15.97
Ti	0.38	0.19
Cr	20.30	9.52
Fe	14.79	6.46
Total	100.00	100.00

Elements	ms%	mol%
O	35.81	61.16
Mg	3.32	3.73
Al	12.11	12.26
Ti	0.41	0.23
Cr	18.31	9.62
Fe	16.38	8.01
As	13.67	4.98
Total	100.00	100.00

Figure 5. Monocrystals of chromite (**left**) and aluminochromite (**center**,**right**).



Elements	ms%	mol%
O	30.61	57.63
Mg	1.71	2.12
Al	3.50	3.91
Ti	0.48	0.30
Cr	42.35	24.53
Fe	21.34	11.51
Total	100.00	100.00

Elements	ms%	mol%
O	32.81	59.48
Mg	2.78	3.31
Al	3.79	4.07
Ti*	0.57	0.34
Cr	41.80	23.31
Fe	18.26	9.48
Total	100.00	100.00

Elements	ms%	mol%
O	30.48	57.94
Mg*	0.68	0.86
Al	3.42	3.86
Ti*	0.50	0.32
Cr	41.31	24.17
Fe	23.61	12.86
Total	100.00	100.00

Figure 6. Deformation of chromite crystal lattice.

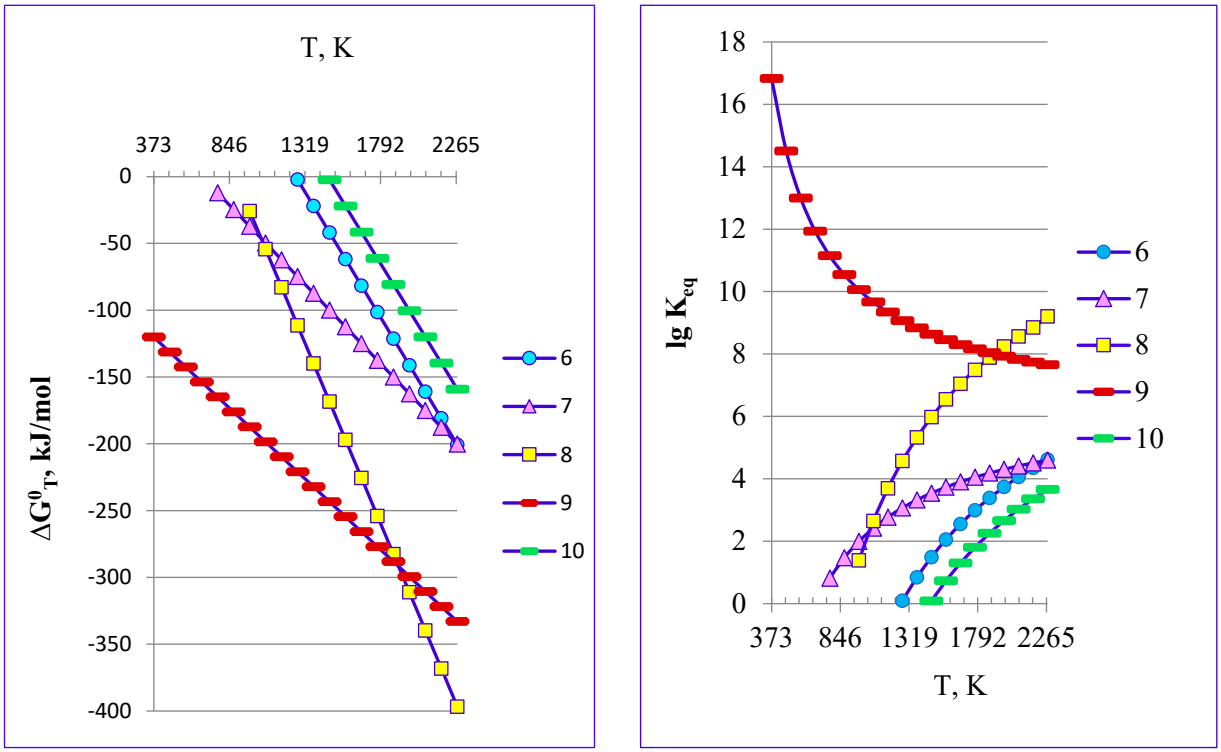
3.2. Mechanism of Oxidizing-Soda Conversion of Ilmenite Concentrate

3.2.1. Thermodynamics of Ilmenite Decomposition Reactions

In chemical processes, two opposing factors—entropic (TΔS) and enthalpic (ΔH)—are known to act simultaneously. The total effect of these opposing factors in processes proceeding at constant pressure and temperature determines the change in Gibbs energy

(ΔG). The nature of the change in the latter allows us to judge the fundamental possibility of the process.

Thermodynamic analysis of reactions of oxidative soda conversion of ilmenite concentrate minerals revealed that the process of ilmenite decomposition by soda ash can proceed at temperatures above 773 K with the formation of ferruginous sodium titanates $NaFeTiO_4$ and $NaFeTi_3O_8$, iron monoxide, sodium trititanate sodium ferrite $Na_2Ti_3O_7$, and the release of carbon dioxide due to the entropic factor of irreversible endothermic Reactions (6)–(8) and (10) with the following numerical values: $\Delta H > 0$, $\Delta S > 0$, $\Delta G < 0$, and $T > \Delta H/\Delta S$ (Figure 7). The formation of ferruginous sodium titanates of the indicated composition during the intermediate stages of ilmenite roasting was found by Abhishek et al. [15].



(**a**) (**b**)

Figure 7. Dependence of ΔG°_T (**a**) and lg K_{eq} (**b**) changes on the temperature of reactions of the oxidative decomposition of ilmenite by soda ash.

$$FeTiO_3 + 0.5Na_2CO_3 + 0.25O_2 \rightarrow NaFeTiO_4 + 0.5CO_2 \uparrow \quad (6)$$

$$3FeTiO_3 + 0.5Na_2CO_3 + 0.25O_2 \rightarrow NaFeTi_3O_8 + 2FeO + 0.5CO_2 \uparrow \quad (7)$$

$$6FeTiO_3 + 3Na_2CO_3 + 1.5O_2 \rightarrow 4NaFeO_2 + 2NaFeTi_3O_8 + 3CO_2 \uparrow \quad (8)$$

$$3FeTiO_3 + 1.5Na_2CO_3 + 0.75O_2 \rightarrow 3NaFeO_2 + 3TiO_2 + 1.5CO_2 \uparrow \quad (9)$$

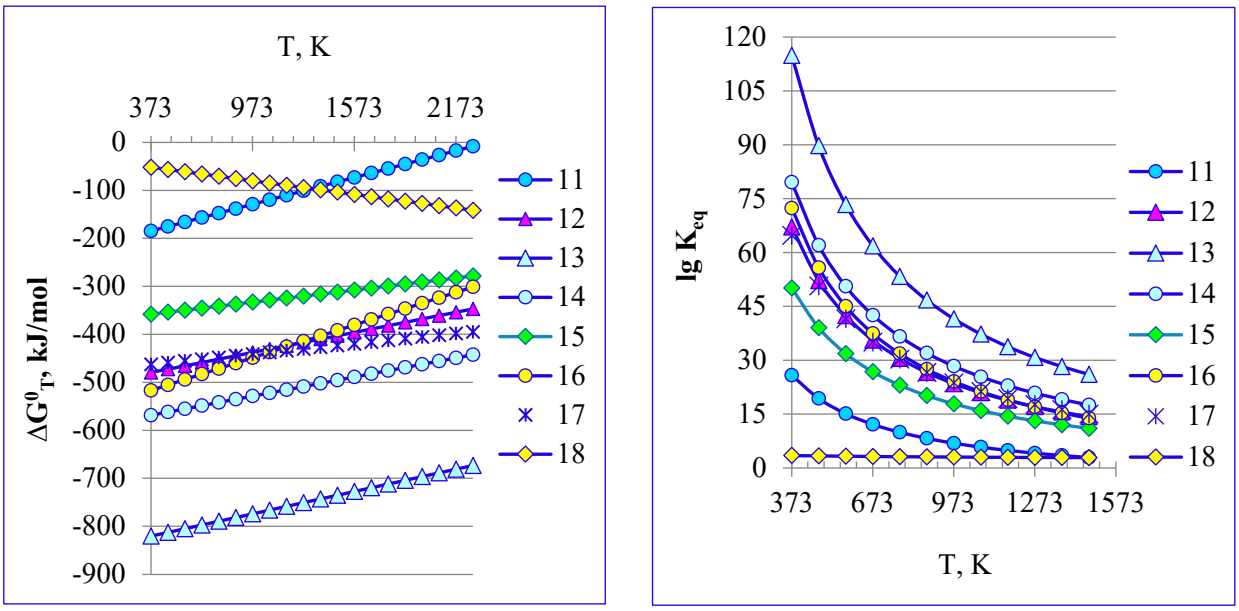
$$3TiO_2 + Na_2CO_3 \rightarrow Na_2Ti_3O_7 + CO_2 \uparrow \quad (10)$$

The endothermic Reaction (9) of ilmenite decomposition with the formation of sodium ferrite and the release of titanium dioxide from the crystal lattice of the mineral under the numerical values $\Delta H > 0$, $\Delta S > 0$, and $\Delta G < 0$ reveals that the initial stage of the sodium trititanate formation process can proceed spontaneously at any temperature, with subsequent heat release. The decomposition of ilmenite, which begins in the low-temperature region, is attributed to the adsorption of oxygen on the mineral surface, leading to the oxidation and transition of divalent iron to the reactive trivalent oxide state, similar to natural conditions. As a result of the interaction of amorphous salt-forming iron trioxide with strongly basic

sodium oxide of soda ash, sodium ferrite is formed. The titanium dioxide released in this process, reacting with sodium oxide, forms sodium trititanate.

It should be explained that sodium oxide is a binary thermally stable, refractory (T_{sinter} 1405 K under high pressure) substance with rigid donor–acceptor bonding of the alkali metal ion with oxygen. Calcined soda is a hygroscopic substance that decomposes upon heating through the absorption of evaporating moisture into sodium oxide and carbon dioxide. The release of carbon dioxide indicates the decomposition of soda ash and the interaction of the mineral and intermediate products of its decomposition with sodium oxide alkaline reagent.

The ilmenite mineral is primarily a metatitanate of iron. The formation of ferric sodium titanates in the low-temperature region is the initial incomplete stage of the gradual decomposition of ilmenite. The possible decomposition of ilmenite using sodium oxide in soda ash to form ferruginous sodium titanate $NaFeTiO_4$ at temperatures ranging from 373 to 773 K, as well as sodium ferrite and ferruginous sodium trititanate $NaFeTi_3O_8$ at temperatures ranging from 373 to 573 K, can proceed due to the enthalpy factor of exothermic Reactions (11) and (12). These reactions are characterized by the following numerical values: $\Delta H < 0$, $\Delta S < 0$, $\Delta G < 0$, and $T < \Delta H/\Delta S$. At temperatures above 773 K and 573 K, the decomposition process of ilmenite can proceed spontaneously due to the dominant ($\Delta S > 0$) entropic factor (Reactions (11) and (12), Figure 8).



(**a**) (**b**)

Figure 8. Dependence of ΔG°_T (**a**) and lg K_{eq} (**b**) changes on the temperature of oxidative decomposition reactions of ilmenite by sodium oxide with soda ash.

$$2FeTiO_3 + Na_2O + 0.5O_2 \rightarrow 2NaFeTiO_4 \quad (11)$$

$$3FeTiO_3 + 1.5Na_2O + 0.75O_2 \rightarrow 2NaFeO_2 + NaFeTi_3O_8 \quad (12)$$

$$2FeTiO_3 + 4Na_2O + 0.5O_2 \rightarrow 2NaFeO_2 + Na_2TiO_3 + Na_4TiO_4 \quad (13)$$

$$3FeTiO_3 + 2.5Na_2O + 0.75O_2 \rightarrow 3NaFeO_2 + Na_2Ti_3O_7 \quad (14)$$

$$2FeTiO_3 + Na_2O + 0.5O_2 \rightarrow 2NaFeO_2 + 2TiO_2 \quad (15)$$

$$3FeTiO_3 + 1.5Na_2O + 0.75O_2 \rightarrow 3NaFeO_2 + 3TiO_2 \quad (16)$$

$$2TiO_2 + 3Na_2O \rightarrow Na_2TiO_3 + Na_4TiO_4 \quad (17)$$

$$3TiO_2 + Na_2O \rightarrow Na_2Ti_3O_7 \quad (18)$$

The decomposition of ilmenite using sodium oxide from soda ash to form sodium ferrite, meta-, ortho-, and trititanates is reflected in exothermic Reactions (13)–(18). Overall, Reactions (13) (formation of sodium ferrite, meta- and ortho-titanates) and 14 (sodium ferrite and trititanate) and intermediate Reactions (15) and (16) (formation of sodium ferrite and titanium dioxide) proceed due to the enthalpic factor, with numerical values of $\Delta H < 0$, over the entire temperature range from 373 to 2273 K. The reactions have $\Delta S < 0$ from 373 to 573 K and from 373 to 473 K, with $\Delta G < 0$ and $T < \Delta H/\Delta S$, and proceed spontaneously at temperatures above 573 and 473 K. The numerical values are $\Delta H < 0$, $\Delta S < 0$, and $\Delta G < 0$ in the whole temperature range and $T < \Delta H/\Delta S$ in Reaction (17), which completes the general reaction of ilmenite decomposition, allowing us to determine that the formation of sodium meta- and orthotitanates in the interaction of the two released moles of titanium dioxide with three moles of sodium oxide proceeds due to the enthalpic factor. The numerical values of $\Delta H < 0$, $\Delta S > 0$, and $\Delta G < 0$ throughout the entire temperature range of Reaction (18), which completes the general Reaction (14) of ilmenite decomposition, indicate that the formation of sodium trititanate in the interaction of three moles of titanium dioxide with one mole of sodium oxide proceeds spontaneously at any temperature.

Thus, via the thermodynamic analysis of chemical reactions, we have determined the temperature range relating to the formation of ferruginous sodium titanates at the decomposition of ilmenite. However, the formation of ferruginous sodium titanates at the initial stage of ilmenite decomposition is possible only in the presence of sodium ions in the reaction mixture of initial substances. Sodium oxide, formed during the decomposition of soda, as mentioned above, is a binary thermally stable, refractory (T_{sinter} 1405 K under high pressure) substance possessing a rigid donor–acceptor bond of the alkali metal ion, i.e., Na+, with oxygen. Through the use of thermodynamic calculations, we have established that sodium oxide derived from soda does not decompose into sodium ions across the wide temperature range of 373 to 2273 K (Appendix B). This is convincing evidence in terms of refuting the existing idea that ilmenite decomposes as a result of the diffusion of iron ions from the crystal lattice of the mineral and the diffusion of sodium ions into the crystal lattice of the mineral. The true mechanism of ilmenite decomposition is logically explained by the oxidation of divalent iron by oxygen and its transition to the trivalent reactive oxide state, which forms water-soluble sodium ferrite when interacting with strongly basic soda sodium oxide, which is reflected in the course of thermodynamic Reactions (13)–(16) shown in Figure 8.

3.2.2. Thermodynamics of Pseudorutile Decomposition Reactions

Pseudorutile $Fe_2Ti_3O_9$, having in its composition trivalent iron oxide in contrast to ilmenite, can be catalytically decomposed without oxygen under the action of sodium oxide with the formation of sodium ferrite and metatitanate in the whole temperature range from 373 to 2273 K due to the enthalpic factor (Figure 9, general exothermic Reaction (19)).

$$Fe_2Ti_3O_9 + 4Na_2O \rightarrow 2NaFeO_2 + 3Na_2TiO_3 \quad (19)$$

$$Fe_2Ti_3O_9 + Na_2O \rightarrow 2NaFeO_2 + 3TiO_2 \quad (20)$$

$$3TiO_2 + 3Na_2O \rightarrow 3Na_2TiO_3 \quad (21)$$

$$Fe_2Ti_3O_9 + 4Na_2CO_3 = 2NaFeO_2 + 3Na_2TiO_3 + 4CO_2 \quad (22)$$

$$3TiO_2 + 3Na_2CO_3 = 3Na_2TiO_3 + 3CO_2 \quad (23)$$

The decomposition of this mineral to form sodium ferrite and titanium dioxide directly can proceed spontaneously at any temperature (initial Reaction (20)). The released titanium dioxide, reacting with sodium oxide, forms sodium metatitanate due to the enthalpic factor (Reaction (21), completing the general Reaction (19)). The destruction of the mineral by soda ash with the formation of sodium ferrite and sodium metatitanate, beginning at 873 K, can occur in the high-temperature region during thermal decomposition of the alkaline reagent,

accompanied by the release of carbon dioxide, due to the entropic factor (endothermic Reactions (22) and (23)).

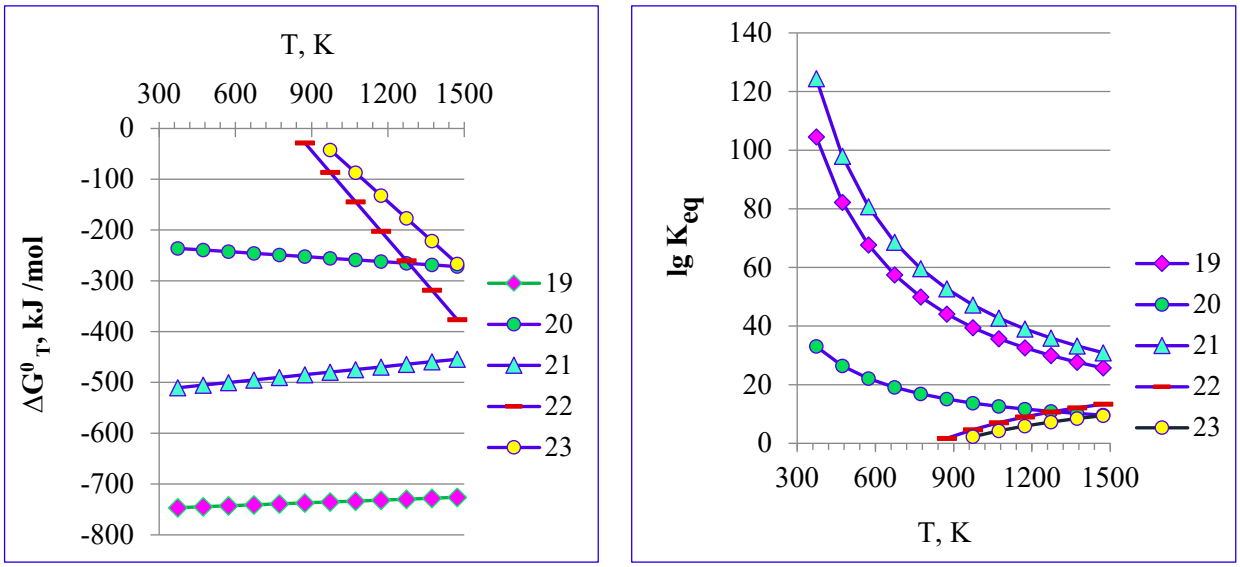


Figure 9. Dependence of ΔG°_{T} (**a**) and lg K_{eq} (**b**) on the temperature of decomposition reactions of pseudorutile by sodium oxide and soda ash.

3.2.3. Thermodynamics of Pseudobrookite Decomposition Reactions

The constituent component of pseudobrukite $Fe_2(TiO_5)$ is reactive trivalent iron oxide; therefore, this allotropic ilmenite mineral, like pseudorutile, can be catalytically decomposed without oxygen at low temperatures by sodium soda oxide, leading to the formation of ferrite and then sodium metatitanate, due to the enthalpy factor of general exothermic Reaction (24), initial spontaneous Reaction (25), and final enthalpy Reaction (26) (Figure 10).

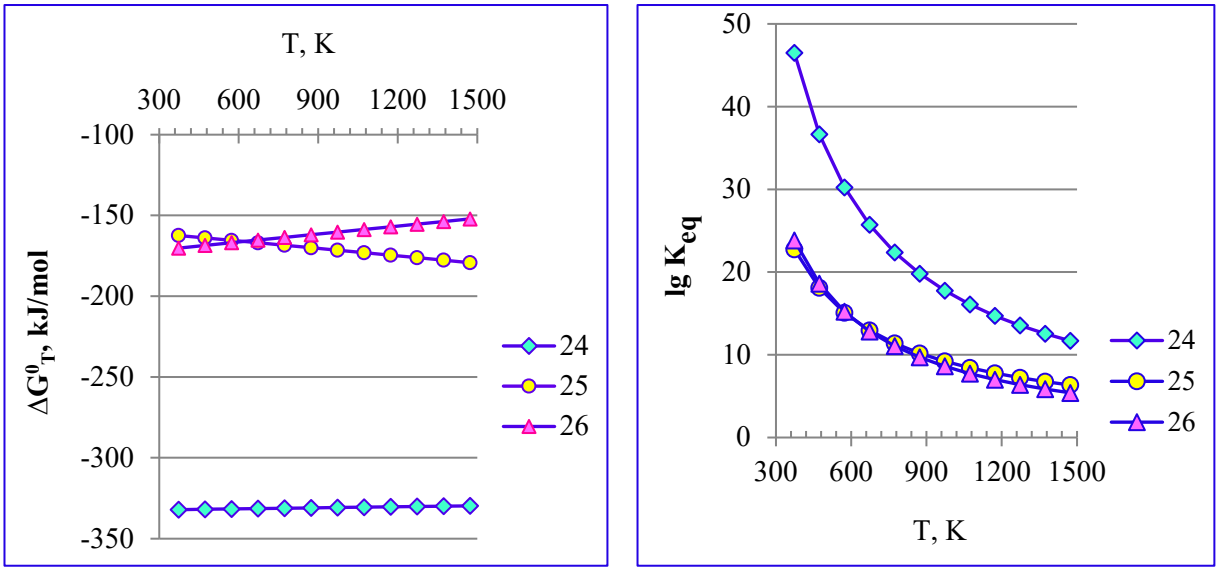


Figure 10. Dependence of ΔG°_{T} (**a**) and lg K_{eq} (**b**) change on the temperature of the decomposition reaction of pseudobrookite by sodium oxide of soda ash.

$$Fe_2(TiO_5) + 2Na_2O \rightarrow 2NaFeO_2 + Na_2TiO_3 \quad (24)$$

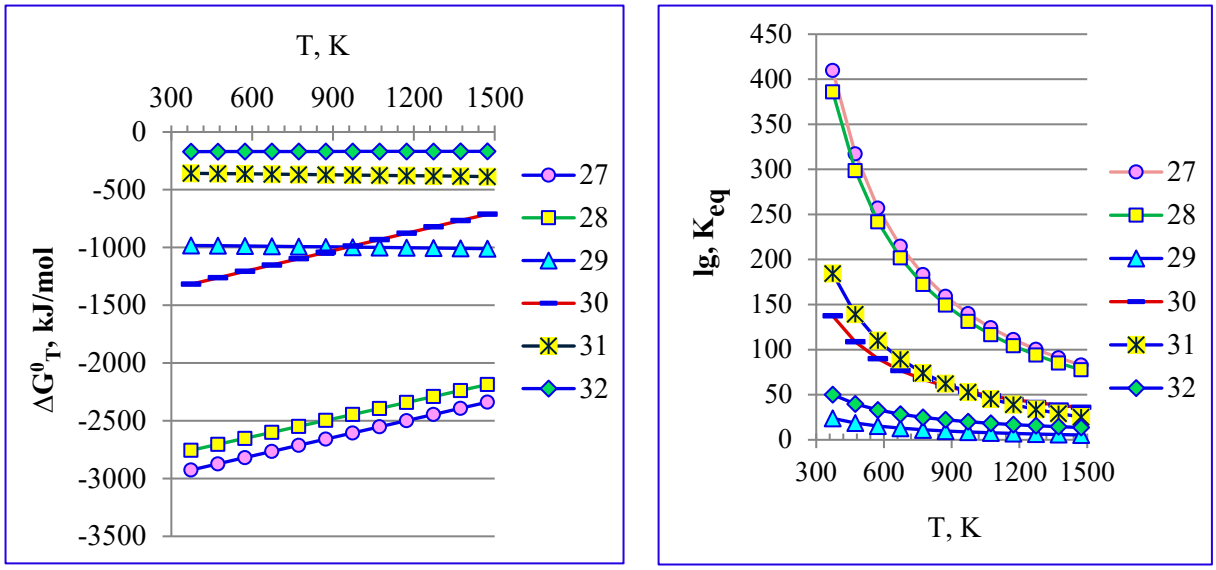
$$Fe_2(TiO_5) + Na_2O \rightarrow 2NaFeO_2 + TiO_2 \quad (25)$$

$$TiO_2 + Na_2O \rightarrow Na_2TiO_3 \quad (26)$$

The hypothetically possible destruction of pseudobrookite by soda ash, starting at 973 K, can proceed in the high-temperature region due to the entropic thermal decomposition of the alkaline reagent accompanied by the release of carbon dioxide.

3.2.4. Thermodynamics of Titanium Disilicide Decomposition Reactions

Titanium disilicide $TiSi_2$—zhiqinite can decompose into constituent oxides spontaneously in the whole studied temperature range (Figure 11, exothermic initial Reaction (27)).



(**a**) (**b**)

Figure 11. Dependence of ΔG°_T (**a**) and lg K_{eq} (**b**) change on the reaction temperature oxidative decomposition of titanium disilicide by sodium oxide of soda ash.

$$TiSi_2 + 2O_2 \rightarrow 2SiO + TiO_2 \quad (27)$$

$$2SiO + O_2 \rightarrow 2SiO_2 \quad (28)$$

$$2SiO_2 + 2Na_2O \rightarrow 2Na_2SiO_3 \quad (29)$$

$$TiSi_2 + 3O_2 + 2Na_2O \rightarrow 2Na_2SiO_3 + TiO_2 \quad (30)$$

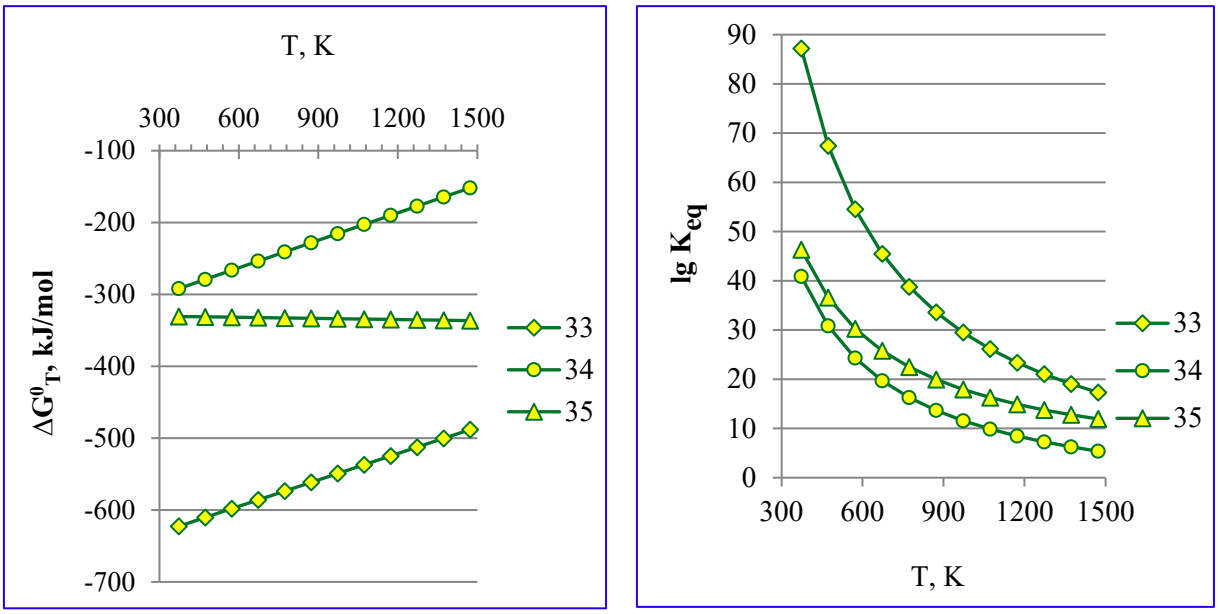
$$TiO_2 + Na_2O \rightarrow Na_2O{\cdot}TiO_2 \quad (31)$$

$$TiSi_2 + 3O_2 + 3Na_2O \rightarrow 2Na_2SiO_3 + Na_2O{\cdot}TiO_2 \quad (32)$$

The destruction of titanium disilicide at low temperatures is promoted via the oxidation and transition of divalent silicon into a reactive strongly acidic dioxide state, actively reacting with strongly basic sodium oxide, proceeding with the formation of sodium metasilicate in the temperature range from 337 to 2273 K due to the enthalpic factor (intermediate exothermic Reactions (28) and (29)). At the same time, the interaction of releasing titanium dioxide with sodium oxide to form sodium metatitanate also occurs in the temperature range from 337 to 2273 K due to the enthalpic factor (subsequent exothermic Reactions (30) and (31), completing the overall Reaction (32)). Probable reactions of metasilicate and sodium metatitanate formation collectively reflect the enthalpic character of the process of oxidative conversion of titanium disilicide by sodium oxide of soda ash.

3.2.5. Thermodynamics of Chromite Decomposition Reactions

The mineral chromite $FeCr_2O_4$, the constituent component of which is divalent iron oxide—which, in contrast to stable reactive trivalent iron oxide, has a smaller charge and a larger ionic radius [22]—can be decomposed by sodium soda ash oxide with the formation of sodium ferrite and sodium metachromite at temperatures ranging from 373 to 573 K due to the enthalpic factor, and spontaneously above 573 K (Figure 12, exothermic general Reaction (33)).



(**a**) (**b**)

Figure 12. Dependence of ΔG°_T (**a**) and lg K_{eq} (**b**) on the temperature of reactions of oxidative decomposition of chromite by sodium oxide with soda ash.

$$2FeCr_2O_4 + 0.5O_2 + 3Na_2O \rightarrow 2NaFeO_2 + 4NaCrO_2 \quad (33)$$

$$2FeCr_2O_4 + 0.5O_2 + Na_2O \rightarrow 2NaFeO_2 + 2Cr_2O_3 \quad (34)$$

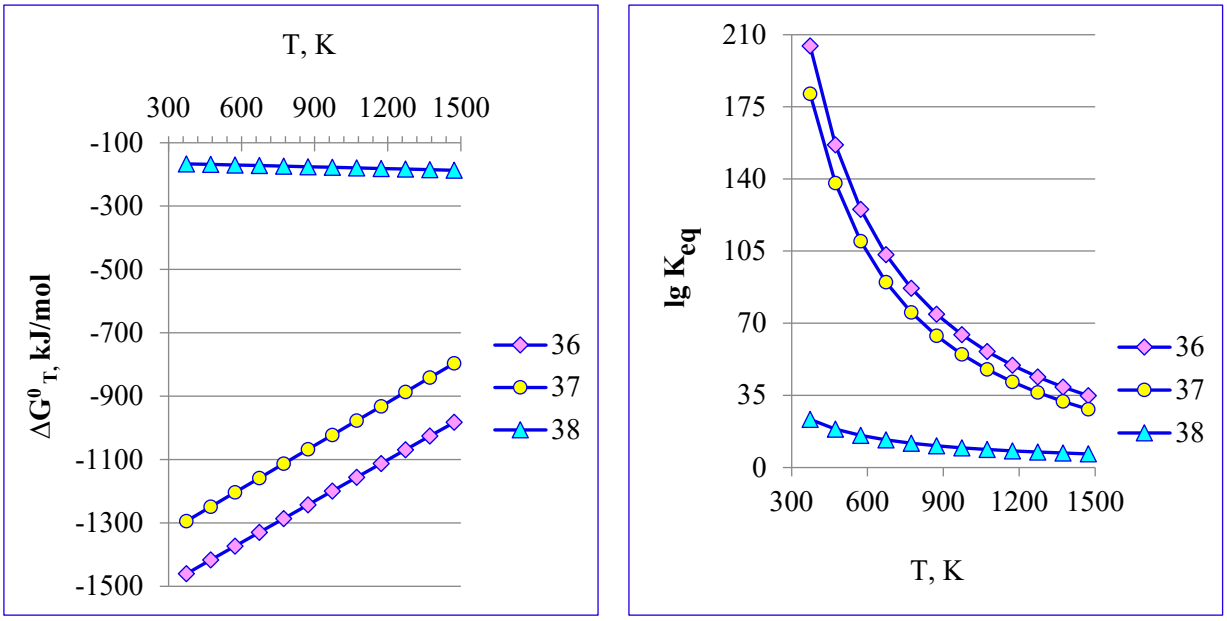
$$2Cr_2O_3 + 2Na_2O \rightarrow 4NaCrO_2 \quad (35)$$

The enthalpic nature of the process of chromite decomposition in the low-temperature region is driven by the initial stage of mineral destruction, which is stimulated by the oxidation and transition of divalent iron into the reactive trioxide state. This reactive iron then reacts strongly with basic sodium oxide to form sodium ferrite and release chromium trioxide (initial exothermic Reaction (34)). The process of oxidative conversion of chromite acquires a spontaneous character as a result of the subsequent spontaneous interaction of chromium trioxide, which is resistant to oxidation, with sodium oxide of soda ash, proceeding with the formation of sodium metachromite (exothermic Reaction (35)), completing general Reaction (33).

3.2.6. Thermodynamics of Spessartine Decomposition Reactions

Spessartine $Mn_3Al_2[SiO_4]_3$—non-silicate manganese-aluminum garnet—is one of many rock-forming vein minerals found as phenocrysts in ilmenite concentrate. The destructive effect on spessartine at low temperatures is exerted by the oxygen and sodium oxide of soda ash. Strongly basic divalent manganese, which is present in the mineral composition, shows great stability, and is easily oxidized by oxygen, acquires an acid trioxide state, forming water-soluble sodium manganate in the process of firing with strongly basic sodium oxide [23]. It is quite possible that the degradation of spessartine is accompanied by the simultaneous interaction of reactive strongly acidic silicon dioxide with

strongly basic sodium oxide to form water-soluble sodium metasilicate. The calculation of the Gibbs energy change in the reaction of oxidative-soda conversion of spessartine is presented in Appendix A. The decomposition of spessartine, which proceeds with the formation of sodium manganate and metasilicate and the release of amorphous aluminum oxide, is driven by the enthalpic factor and is represented by exothermic Reaction (37) (Figure 13).



(**a**) (**b**)

Figure 13. Dependence of change in ΔG°_{T} (**a**) and lg K_{eq} (**b**) on the temperature of oxidative decomposition reactions of spessartine by sodium oxide of soda ash.

$$Mn_3Al_2[SiO_4]_3 + 3O_2 + 7Na_2O \rightarrow 3Na_2MnO_4 + 3Na_2SiO_3 + 2NaAlO_2 \quad (36)$$

$$Mn_3Al_2[SiO_4]_3 + 3O_2 + 6Na_2O \rightarrow 3Na_2MnO_4 + 3Na_2SiO_3 + Al_2O_3 \quad (37)$$

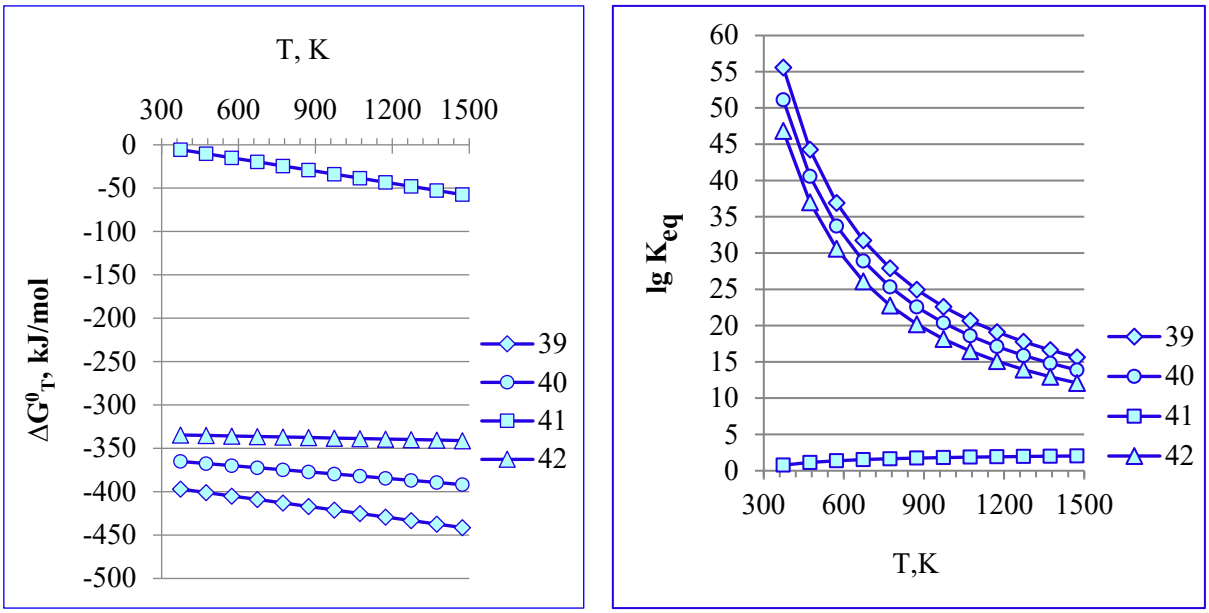
$$Al_2O_3 + Na_2O \rightarrow 2NaAlO_2 \quad (38)$$

Amorphous aluminum oxide can interact with strongly basic sodium oxide spontaneously over the entire temperature range to form water-soluble sodium aluminate after sodium oxide binds reactive strongly acidic manganese and silicon oxides (exothermic Reaction (38), completing the general Reaction (36) of spessartine decomposition).

3.2.7. Thermodynamics of Zircon Decomposition Reactions

Metamict zircon $ZrSiO_4$, found in ilmenite concentrate, is a very hard (7.5 Mohs slag) mineral of the subclass of island silicates, consisting of reactive strongly acidic silicon dioxide and extremely refractory zirconium dioxide (T_{sinter}. 2715 °C), which is almost 1.5 times stronger than titanium dioxide (T_{sinter}. 1843 °C).

Due to the active reaction properties of silicon dioxide and sodium oxide of soda ash, zirconium orthosilicate can spontaneously decompose across the entire temperature range, forming sodium metasilicate and releasing zirconium dioxide mineral from the crystal lattice (Figure 14, initial exothermic Reactions (40) and (41)).



(**a**) (**b**)

Figure 14. Dependence of change in $\Delta G^{\circ}{}_T$ (**a**) and lg K_{eq} (**b**) on the temperature of reactions of zircon decomposition by sodium oxide of soda ash.

$$ZrSiO_4 + 3Na_2O \rightarrow Na_4SiO_4 + Na_2ZrO_3 \quad (39)$$

$$ZrSiO_4 + 2Na_2O \rightarrow Na_4SiO_4 + ZrO_2 \quad (40)$$

$$SiO_2 + 2Na_2O \rightarrow Na_4SiO_4 \quad (41)$$

$$ZrO_2 + Na_2O \rightarrow Na_2ZrO_3 \quad (42)$$

The interaction of amorphous zirconium dioxide with sodium oxide of soda ash, in accordance with its stability, can proceed with the formation of sodium zirconate due to the entropic factor of exothermic Reaction (42), which completes the general Reaction (39), reflecting the spontaneous character of the exothermic decomposition of zircon.

3.3. Evaluation of the Efficiency of Oxidizing Soda Conversion of Polymineral Ilmenite Concentrate

As a result of the thermodynamic analysis of the chemical reactions, a one-stage oxidizing soda conversion of ilmenite concentrate was developed. As a result of testing technological conditions, samples of synthetic rutile were obtained. The composition is presented in Figure 15 and Table 5. The quality of the synthetic rutile samples was estimated at the Central Laboratory of Kazakhstani Ust-Kamenogorsk titanium-magnesium combine (JSC "UK TMC"), certified by the PRI (USA) in terms of conformity to international standards "Nadcap".

The specified technological mode of the roasting process ensures the completeness of decomposition of all minerals, and the refining of concentrate cinders achieves efficient purification of titanium dioxide from easily soluble sodium salts of accompanying elements.

The chemical composition of a representative sample of synthetic rutile (in wt%) was as follows: TiO_2—96.516; Fe_2O_3—0.185; Cr_2O_3—0.249; SiO_2—1.237; Al_2O_3—0.839; ZrO_2—0.343; MgO—0.017; P_2O_5—0.201; Nb_2O_5—0.081; Y_2O_3—0.005; and CaO—0.033.

Further studies determined the feasibility of regenerating soda and carbonizing alkaline filtrate through water-refining the concentrate cinders; this process yields amorphous silica and sodium bichromate. Additionally, hydrochloric acid evaporation of the acidic filtrate of the pulp in the evaporator columns with the condensation of hydrogen chloride results in the production of an iron oxide pigment.

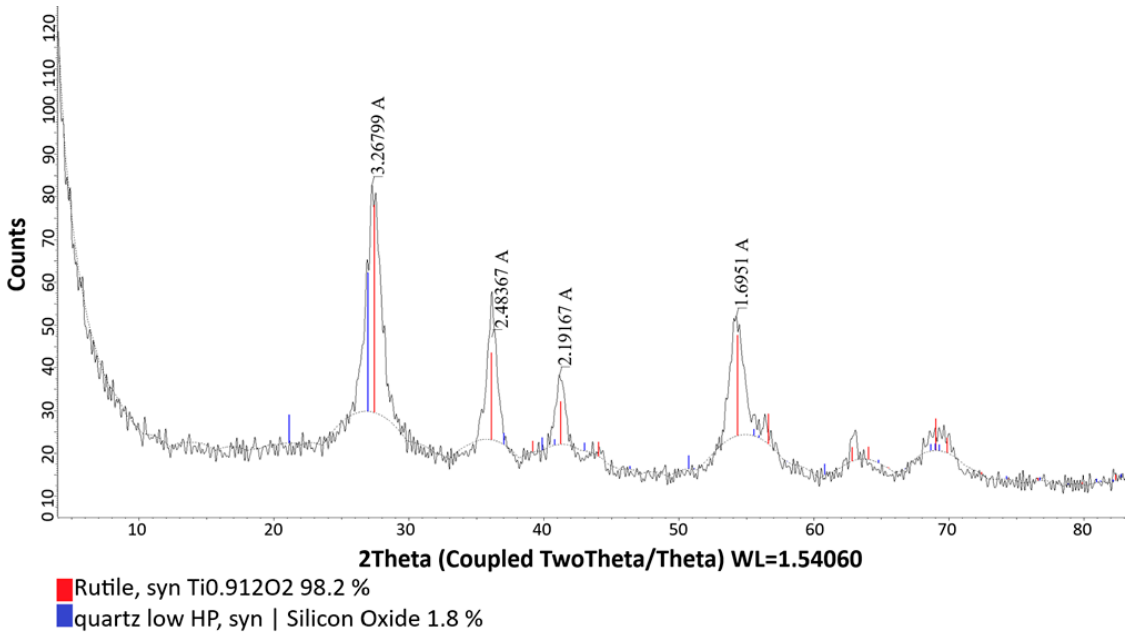


Figure 15. X-ray diffraction of a representative sample of synthetic rutile.

Table 5. Quality of a representative sample of synthetic rutile, according to the results of X-ray phase analysis.

Name	Formula	%
Rutile, syn	$Ti_{0.912}O_2$	98.2
Silicon Oxide	SiO_2	1.8

4. Conclusions

1. The thermodynamic parameters of simple and complex minerals, which are absent in the reference literature, can be determined using the incremental Kumok method, the additive Neumann–Kopp rule, and the Mostafa group contribution method;
2. The stability of ilmenite concentrate minerals depends on the oxidation degree and the reaction properties of structural metal and silicon oxides. The oxides of iron (III), silicon (IV), and manganese (VI) have the best reactivity in solid-phase oxidizing–alkaline medium;
3. The destructive effect on the minerals of ilmenite concentrate is exerted by air oxygen and sodium oxide of soda ash, decomposing in the low-temperature region by absorbing heat and evaporating moisture in the process of dehydrating goethite, lepidocrocite, manganite, and clay minerals and dehydration via heating briquetted soda charge concentrate with an aqueous binder solution;
4. The oxidative soda conversion mechanism of ilmenite concentrate is explained by the decomposition of ilmenite, zhikinite, chromite, and spessartine by air oxygen and the transition of iron, silicon, and manganese from the lowest divalent to the reactive oxide state reacting with strongly basic sodium soda oxide to form ferrite, inert sodium titanates, metasilicate, manganate, metachromite, and sodium aluminate. For pseudorutile and pseudobrukite, due to the presence of reactive iron trioxide and zircon in the structure, strongly acid-reactive silicon dioxide catalytically decomposes strongly basic sodium soda oxide without the participation of oxygen to form first ferrite and metasilicate and then meta-titanate and sodium zirconate;
5. The one-stage soda conversion of high-chromium, silica, rutilized and leucoxene ilmenite concentrates via air oxygen with the subsequent refining of concentrate cinder with water, followed by diluted hydrochloric acid, simplifies the process of

obtaining high-purity synthetic rutile and reduces the cost of producing metallic titanium and titanium pigments.

Author Contributions: K.A.: project administration, writing—original draft preparation, writing—review and editing, N.T.: conceptualization, methodology, and writing—review and editing, B.K.: methodology; S.G.: methodology, N.A.: methodology and writing—review and editing; L.I.: formal analysis. All authors have read and agreed to the published version of the manuscript.

Funding: This research was funded by the Science Committee of the Ministry of Science and Higher Education of the Republic of Kazakhstan (Grant No. AP19677721).

Data Availability Statement: The original contributions presented in the study are included in the article; further inquiries can be directed to the corresponding author.

Conflicts of Interest: The authors declare no conflicts of interest.

Appendix A

Calculation of the Gibbs energy change in the oxidative soda conversion reaction of spessartine $Mn_3Al_2[SiO_4]_3$.

		$Mn_3Al_2[SiO_4]_3$ + $3O_2$ +$7Na_2O$ = $3Na_2MnO_4$ + $2NaAlO_2$ + Na_2SiO_3					
		−5,551,450	0	−430,600	−1,134,110	−1,133,000	−1,554,000
		345.86	205	71.1	176.02	70.71	114.80
		336.72	29.36	72.43	149.72	73.3	111.88
				1 approx.		2 approx.	
H, J	−1,764,680	t, C	T, K	G, kJ	H, J	S	G, kJ
S	−444.68	100	373	−1598.81	−1,764,711.0	−444.8	−1598.8
Cp	−0.413	200	473	−1554.35	−1,764,752.3	−444.9	−1554.3
		300	573	−1509.88	−1,764,793.6	−445.0	−1509.9
		400	673	−1465.41	−1,764,834.9	−445.0	−1465.4
		500	773	−1420.94	−1,764,876.2	−445.1	−1420.9
		600	873	−1376.47	−1,764,917.5	−445.1	−1376.4
		700	973	−1332.01	−1,764,958.8	−445.2	−1331.9
		800	1073	−1287.54	−1,765,000.1	−445.2	−1287.5
		900	1173	−1243.07	−1,765,041.4	−445.2	−1243.0
		1000	1273	−1198.60	−1,765,082.7	−445.3	−1198.5
		1100	1373	−1154.13	−1,765,124.0	−445.3	−1154.0
		1200	1473	−1109.67	−1,765,165.3	−445.3	−1109.6
		1300	1573	−1065.20	−1,765,206.6	−445.4	−1065.1
		1400	1673	−1020.73	−1,765,247.9	−445.4	−1020.6
		1500	1773	−976.26	−1,765,289.2	−445.4	−976.1
		1600	1873	−931.79	−1,765,330.5	−445.4	−931.7
		1700	1973	−887.33	−1,765,371.8	−445.5	−887.2
		1800	2073	−842.86	−1,765,413.1	−445.5	−842.7
		1900	2173	−798.39	−1,765,454.4	−445.5	−798.2
		2000	2273	−753.92	−1,765,495.7	−445.5	−753.7

Calculation of the Gibbs energy change is carried out in two approximations. In the first approximation, it is assumed that $\Delta C_P^\circ = 0$; then,

$$\Delta G_T^\circ = \Delta H_{298}^\circ - T\Delta S_{298}^\circ \quad \text{(A1)}$$

Using this equation gives satisfactory results if ΔC_P° in the reaction is small.
In the second approximation, it is assumed that $\Delta C_P^\circ = \text{const} = \Delta C_{298}^\circ$; then,

$$\Delta H^\circ{}_T = \Delta H^\circ{}_{298} + \Delta C^\circ{}_{p,298}(T - 298) \quad \text{(A2)}$$

$$\Delta S^\circ{}_T = \Delta S^\circ{}_{298} + \Delta C^\circ{}_{p,298} \ln\left(\frac{T}{298}\right) \quad \text{(A3)}$$

$$\Delta G^{\circ}{}_T = \Delta H^{\circ}{}_T - T\Delta S^{\circ}{}_T \quad \text{(A4)}$$

In the third approximation, the change in heat capacity ΔC_P° is calculated as a function of temperature:

$$\Delta H^{\circ}{}_T = \Delta H^{\circ}{}_{298} + \Delta a(T - 298) + \frac{\Delta b}{2}\left(T^2 - 298^2\right) - \Delta c'\left(\frac{1}{T} - \frac{1}{298}\right) \quad \text{(A5)}$$

$$\Delta S^{\circ}{}_T = \Delta S^{\circ}{}_{298} + \Delta a * ln\left(\frac{T}{298}\right) + \Delta b(T - 298) - \frac{\Delta c'}{2}\left(\frac{1}{T^2} - \frac{1}{298^2}\right) \quad \text{(A6)}$$

$$\Delta G^{\circ}{}_T = \Delta H^{\circ}{}_T - T\Delta S^{\circ}{}_T \quad \text{(A7)}$$

The above formulas in two approximations were entered into Excel, and calculations were performed. Close Gibbs energy values were obtained in the second and third approximations.

Due to the absence of the standard thermodynamic values ΔH_{298}°, ΔS_{298}°, and ΔC_{298}° for some minerals, such as spessartine ($Mn_3Al_2[SiO_4]_3$), pseudorutile ($Fe_2Ti_3O_9$), and pseudobrukite ($FeTi_2O_5$) in the reference literature, these values were determined using the additive Neumann–Kopp rule, Kumok's incremental method, and Mostafa's group contribution method.

Thermodynamic calculations of chemical reactions were also calculated using the HSC Chemistry 8.0 program (2014) for additional verification.

The Neumann–Kopp additive rule allows the thermodynamic values of a complex compound to be calculated by summing simple compound oxides:

$$\Delta H_{298}^{o}(B) = \sum n_i \Delta H_{298}^{o}(i), \quad \text{(A8)}$$

where $\Delta H_{298}^{o}(i)$, n_i is the standard enthalpy and number of moles of the *i*-th compound in complex B compounds.

$$S_{298}^{o}(B) = \sum n_i S_{298}^{o}(i), \quad \text{(A9)}$$

where $S_{298}^{o}(i)$, n_i is thestandard enthalpy and number of moles of the *i*-th compound in complex B compounds.

$$C_{P,298}^{o}(B) = \sum n_i C_{P,298}^{o}(i), \quad \text{(A10)}$$

where $C_{P,298}^{o}(i)$, n_i is the standard heat capacity and number of moles of the *i*-th compound in the complex B compounds.

For example, to calculate the standard thermodynamic values of spessartine $Mn_3Al_2[SiO_4]_3$, the formula of this mineral can be rewritten in the following oxide form: $3MnO \cdot AI_2O \cdot 3SiO_2$. Let us use the additive Neumann–Kopp rule to calculate the standard values of spessartine using Formulas (A8)–(A10):

$$\Delta H_{298} = 3 \times \Delta H_{298}\,(MnO) + \Delta H_{298}\,(AI_2O_3) + 3 \times \Delta H_{298}\,(SiO_2) = 3 \times (-385220) + (-1675690) + 3 \times (-912000) = -5461950\ J/mol.$$

$$\Delta S_{298} = 3 \times \Delta S_{298}\,(MnO) + \Delta S_{298}\,(AI_2O_3) + 3 \times \Delta S_{298}\,(SiO_2) = 3 \times 59.71 + 50.95 + 3 \times 42.09 = 356.35\ J/mol{\cdot}K.$$

$$\Delta C_{P\,298} = 3 \times \Delta C_{P,298}\,(MnO) + \Delta C_{P,298}\,(AI_2O_3) + 3 \times \Delta C_{P,298}\,(SiO_2) = 345.1\ J/mol{\cdot}K.$$

Incremental Kumok method (IKM) calculations were carried out according to the following formulas:

$$\Delta H_{298}^{o}(B) = \Delta H_K{\cdot}n_K + \Delta H_A{\cdot}n_A, \quad \text{(A11)}$$

where n_K and n_A are the number of cations and anions, and ΔH_K and ΔH_A are the increments of cations and anions, respectively.

$$S_{298}^{o}(B) = \Delta S_K{\cdot}n_K + \Delta S_A{\cdot}n_A, \quad \text{(A12)}$$

where n_K and n_A represent the number of cations and anions, and ΔS_K and ΔS_A represent the increments of cations and anions, respectively.

$$C^o_{P,298}(B) = C^o_{P,298}(K) \cdot n(K) + C^o_{P,298} \cdot n(A) \quad \text{(A13)}$$

where (B) is the complex compound or mineral, n(K) and n(A) are the number of cations (K) and anions (A), and $C^o_{P,298}(K)$ and $C^o_{P,298}(A)$ are the increments of cations and anions, respectively.

The standard enthalpy of formation can be calculated using Mostafa's group contribution method:

$$\Delta H^o_{298} = \sum_i n_i \Delta H_i$$

where n_i represents the stoichiometric coefficients of the i-th atom of the compound, and ΔH_i represents the enthalpic increment of the i-th atom.

Tables A1–A3 summarize the results of the calculation of standard thermodynamic quantities of spessartine via different methods.

Table A1. Calculated values ΔH^o_{298} (spessartine) (kJ/mol) using different model equations.

Name	ΔH_{298} (1) Neumann–Kopp Method	ΔH_{298} (4) Kumok Method	ΔH_{298} (Average)
Spessartine $Mn_3Al_2[SiO_4]_3$	5409.25	5693.65	5551.45

Table A2. Calculated values ΔS^o_{298}(spessartine) (J/mol·K) using different model equations.

Name	ΔS_{298} (1) Neumann–Kopp Method	ΔS_{298} (5) Kumok Method	ΔS_{298} (Average)
Spessartine $Mn_3Al_2[SiO_4]_3$	356.35	345.1	345.86

Table A3. Calculated values $\Delta C^o_{P,298}$(spessartine) (J/mol·K) using different model equations.

Name	$\Delta C_{p,298}$ (1) Neumann–Kopp Method	$\Delta C_{P,298}$ (6) Kumok Method	$\Delta C_{P,298}$ (Average)
Spessartine $Mn_3Al_2[SiO_4]_3$	338.06	335.38	336.72

Thermodynamic parameters of pseudorutile—$Fe_2Ti_3O_9$ and pseudobrukite $FeTi_2O_5$—were determined using similar calculations.

Appendix B

Via the thermodynamic analysis of chemical reactions, we determined the temperature range of the formation of ferruginous sodium titanates in the process of ilmenite decomposition. However, the formation of ferruginous sodium titanates in the initial stage of ilmenite decomposition is only possible if a sodium ion is present in the reaction mixture of the initial substances. Sodium oxide, formed during the decomposition of soda, is known to be a binary thermally stable, refractory (T_{smelt}. 1405 K under high pressure) substance possessing a rigid donor–acceptor bond between sodium ions and oxygen. Via thermodynamic calculations, we found that sodium soda oxide does not decompose into sodium ions in a wide temperature range of 373 to 2273 K, as evidenced by the value of the Gibbs energy.

$2Na_2O = Na_2O_2 + 2Na^+$					
−430,600	−510,900	611,000			
71.1	93.3	148			
72.43	89.33	128.2			
H, J	1,572,300				
S	247.1				
Cp	200.87				
		1 approx.			2 approx.
t, C	T, K	G, kJ	H	S	G, kJ
100	373	1480.13	1,587,365	292.19	1478.4
200	473	1455.42	1,607,452	339.90	1449.2
300	573	1430.71	1627,539	378.43	1419.9
400	673	1406.00	1,647,626	410.74	1390.7
500	773	1381.29	1,667,713	438.57	1361.5
600	873	1356.58	1,687,800	463.00	1332.3
700	973	1331.87	1,707,887	484.79	1303.1
800	1073	1307.16	1,727,974	504.44	1273.8
900	1173	1282.45	1,748,061	522.34	1244.6
1000	1273	1257.74	1,768,148	538.77	1215.4
1100	1373	1233.03	1,788,235	553.96	1186.2
1200	1473	1208.32	1,808,322	568.08	1157.0
1300	1573	1183.61	1,828,409	581.28	1127.7
1400	1673	1158.90	1,848,496	593.66	1098.5
1500	1773	1134.19	1,868,583	605.32	1069.3
1600	1873	1109.48	1,888,670	616.34	1040.1
1700	1973	1084.77	1,908,757	626.79	1010.9
1800	2073	1060.06	1,928,844	636.72	981.7
1900	2173	1035.35	1,948,931	646.18	952.4
2000	2273	1010.64	1,969,018	655.22	923.2

Thermodynamic analysis of the Gibbs energy of the sodium oxide decomposition reaction.

This is convincing evidence refuting the existing idea that ilmenite decomposes as a result of the diffusion of iron ions from the crystal lattice of the mineral and the diffusion of sodium ions into the crystal lattice of the mineral. The true mechanism of ilmenite decomposition is explained by the oxidation of divalent iron by oxygen and its transition to the trivalent reactive oxide state, which forms water-soluble sodium ferrites in interactions with strongly basic soda sodium oxide, which is reflected in the course of thermodynamic Reactions (13)–(16), which are shown in Figure 6.

References

1. Global Titanium Minerals Reserves 2010–2023. Available online: https://www.statista.com/statistics/759972/mine-production-titanium-minerals-worldwide-by-country (accessed on 4 May 2024).
2. Perks, C.; Mudd, G. A detailed assessment of global Zr and Ti production. *Miner. Econ.* **2021**, *34*, 345–370. [CrossRef]
3. Naqrale, P. Titanium Dioxide Market Size & Share/Global Forecast Report 2032. June 2024, p. 185. Available online: https://www.marketresearchfuture.com/reports/titanium-dioxide-market-1081 (accessed on 12 June 2024).
4. Subasinghe, H.C.S.; Ratnayake, A.S. Mechanical activation and physicochemical factors controlling pyrometallurgical, hydrometallurgical and electrometallurgical processing of titanium ore. *J. S. Afr. Inst. Min. Metall.* **2023**, *123*, 399–414. [CrossRef]
5. Nurul, A. Chemical and Electrochemical Leaching Studies of Synthetic and Natural Ilmenite in Hydrochloric Acid Solution. Ph.D. Thesis, Murdoch University, Perth, Australia, 2016.
6. Zhang, W.; Zhu, Z.; Cheng, C.Y. A literature review of titanium metallurgical processes. *Hydrometallurgy* **2011**, *108*, 177–188. [CrossRef]
7. Verhulst, D.; Sabachy, B.; Spitler, T.; Dyuvesteyn, W. The Altair TiO_2 pigment process and its extension into the field of nanomaterials. *CIM Bull.* **2002**, *95*, 89–94.
8. Formanek, L.; Lommert, H.; Beyzavi, A.-N. Synthetic Putile Manufacture by the SL/RN-Becher Process. *Heavy Miner.* **1997**, 161–168.

9. Walpole, E.A.; Winter, J.D. The Austpac ERVS and EARS Processes for the Manufacture of High-Grade Synthetic Rutile by Hydrochloric Asid Leaching of Ilmenite. In Proceedings of the International Conference on the Practice and Theory of Chloride, Metal Interaction, Montreal, QC, Canada, 19–23 October 2002.
10. Zhaowang, D.; Yang, X.; Xueyi, G.; Jinlong, Z.; Linfeng, J.; Linfeng, J.; Qinghua, T.; Yang, L. Direct reduction of upgraded titania slag by magnesium for making low-oxygen containing titanium alloy hydride powder. *Powder Technol.* **2020**, *368*, 160–196.
11. Guéguin, M.; Cardarelli, F. Chemistry and mineralogy of titania-rich slags. Part 1—Hemo-ilmenite, sulphate, and upgraded titania slags. *Miner. Process. Extr. Metall. Rev.* **2007**, *28*, 1–58. [CrossRef]
12. Morsi, I.M.; Abdullah, F.H.A.; Mohamed, O.A.; Shalabi, M.E.H.; El-Tawil, S.Z. Processing of ilmenite ore by sintering/roasting technique. In Proceedings of the 3rd Mining, Petroleum and Metallurgy Conference, Cairo, Egypt, 2–4 February 1992.
13. Lasheen, T.A. Soda ash roasting of titana slag product from Rosetta ilmenite. *Hydrometallurgy* **2008**, *93*, 124–128. [CrossRef]
14. Nafeaa, I.A.; Zekry, A.F.; Khalifa, M.G.; Farag, A.B.; El-Hussiny, N.A.; Shalabi, M.E.H. Kinetics of Reaction of Roasting of Soda Ash and Ilmenite Ore Concentrate for Formation of Sodium Titanates. *Sci. Sinter.* **2015**, *47*, 319–329. [CrossRef]
15. Abhishek, L.; Animesh, J. Kinetics and Reaction Mechanism of Soda Ash Roasting of Ilmenite Ore for the Extraction of Titanium Dioxide. *Metall. Mater. Trans. B* **2007**, *38*, 939–948.
16. Kenzhaliev, B.K.; Akhmetova, K.S.; Trebukhov, S.A.; Gladyshev, S.V.; Tuleutai, F.H.; Zinovieva, L.V. Method of Processing Ilmenite Concentrates. Patent 34030 RK, 26 November 2019.
17. Lidin, L.A.; Andreeva, L.L.; Molochko, V.A. *Constants of Inorganic Substances (Reference Book)*; Drofa: Moscow, Russia, 2008; 685p.
18. Chumilina, L.G.; Belokopytova, D.V.; Denisov, V.M. Calculation of the thermodynamic properties of the $Ca_3R_2Ge_3O_{12}$ germanates (R = Y, Er - Lu). *J. Sib. Fed. Chem.* **2022**, *15*, 409–419. (In Russian)
19. Ivanova, V.P. *Thermal Analysis of Minerals and Rocks*; Nedra: Leningrad, Russia, 1974; 49p. (In Russian)
20. Ramadan, A.M.; Farghaly, M.; Fathy, W.M.; Ahmed, M.M. Leaching and kinetics studies on processing of Abu-Ghalaga ilmenite ore. *Int. Res. J. Eng. Technol. (IRJET)* **2016**, *3*, 46–60.
21. Swanepoel, J.J. Process Development for the Removal of Iron from Nitrided Ilmenite. Master's Thesis, Department of Chemical Engineering Faculty of Engineering, Built Environment & Information Technology, University of Pretoria, Pretoria, South Africa, October 2010; 151p. Submitted in partial fulfilment of the requirements for the degree of Master of Engineing (chem eng).
22. James, E. *Inorganic Chemistry: Principles of Structure and Reactivity*, 3rd ed.; Harper & Row: New York, NY, USA, 1987; p. 698.
23. Ripan, R.; Cheteanu, I. *Inorganic Chemistry. Chemistry of Metals*; Mir: Moscow, Russia, 1972; Volume 2, p. 871. (In Russian)

Disclaimer/Publisher's Note: The statements, opinions and data contained in all publications are solely those of the individual author(s) and contributor(s) and not of MDPI and/or the editor(s). MDPI and/or the editor(s) disclaim responsibility for any injury to people or property resulting from any ideas, methods, instructions or products referred to in the content.